

Probing the 9.7 μm Interstellar Silicate Extinction Profile through the *Spitzer*/IRS Spectroscopy of OB Stars

Zhenzhen Shao^{1,2,3*}, B.W. Jiang^{1†}, Aigen Li^{2‡}, Jian Gao¹, Zhangpan Lv¹, and Jiawen Yao¹

¹*Department of Astronomy, Beijing Normal University, Beijing 100875, China*

²*Department of Physics and Astronomy, University of Missouri, Columbia, MO 65211, USA*

³*Beijing Ancient Observatory, Beijing Planetarium, Beijing 100005, China*

Received date / Accepted date

ABSTRACT

The 9.7 μm interstellar spectral feature, arising from the Si–O stretch of amorphous silicate dust, is the strongest extinction feature in the infrared (IR). In principle, the spectral profile of this feature could allow one to diagnose the mineralogical composition of interstellar silicate material. However, observationally, the 9.7 μm interstellar silicate extinction profile is not well determined. Here we utilize the *Spitzer*/IRS spectra of five early-type (one O- and four B-type) stars and compare them with that of unreddened stars of the same spectral type to probe the interstellar extinction of silicate dust around 9.7 μm . We find that, while the silicate extinction profiles all peak at $\sim 9.7 \mu\text{m}$, two stars exhibit a narrow feature of FWHM $\sim 2.0 \mu\text{m}$ and three stars display a broad feature of FWHM $\sim 3.0 \mu\text{m}$. We also find that the width of the 9.7 μm extinction feature does not show any environmental dependence. With a FWHM of $\sim 2.2 \mu\text{m}$, the mean 9.7 μm extinction profile, obtained by averaging over our five stars, closely resembles that of the prototypical diffuse interstellar medium along the lines of sight toward Cyg OB2 No. 12 and WR 98a. Finally, an analytical formula is presented to parameterize the interstellar extinction in the IR at $0.9 \mu\text{m} \lesssim \lambda \lesssim 15 \mu\text{m}$.

Key words: ISM: dust, extinction – infrared: ISM – infrared: stars – stars: early-type

1 INTRODUCTION

The wavelength dependence of the interstellar extinction, known as the interstellar extinction curve or the interstellar extinction law, varies substantially in the ultraviolet (UV) and optical wavelengths (see Draine 2003). Cardelli et al. (1989; hereafter CCM) found that this variation can be closely parameterized by a single parameter R_V , where the dimensionless quantity $R_V \equiv A_V/(A_B - A_V)$ is the total-to-selective extinction ratio between the B band at $\lambda \approx 4400 \text{ \AA}$ and the V band at $\lambda \approx 5500 \text{ \AA}$. As R_V varies from one region to another, the slope of the UV/optical extinction curve shows considerable variations from being steep in diffuse regions characterized by a smaller R_V (typically $\lesssim 3$) to being flat in regions which are more dense and characterized by a larger R_V (typically $\gtrsim 4$; see Li et al. 2015). The 2175 \AA extinction bump, the strongest spectral feature in the UV extinction curve, also varies with R_V . While the peak wavelength of the 2175 \AA bump is invariant, its width (γ) increases with R_V (see Figure 3.8 of

Whittet 2003) and its height ($\propto \gamma^{-2}$), the excess extinction of the bump over the underlying linear background extinction, decreases with R_V (see Figure 7 of CCM). In contrast, in the near- and mid-infrared wavelength range of $0.9 \mu\text{m} \lesssim \lambda \lesssim 8 \mu\text{m}$, the interstellar extinction curve appears to be remarkably uniform over the sky and shows little variation with R_V (e.g., see Martin & Whittet 1990, Wang & Jiang 2014, Xue et al. 2016).

At $\lambda \gtrsim 8 \mu\text{m}$, the extinction curve exhibits a pronounced spectral feature at $\sim 9.7 \mu\text{m}$, the strongest extinction feature in the IR. This feature is attributed to the Si–O stretching absorption of silicate dust (Henning 2010). In principle, the spectral profile of the 9.7 μm silicate extinction feature allows one to diagnose the mineralogical composition of interstellar silicate material.¹ However, observationally, the spectral profile of the 9.7 μm silicate extinction is not as well determined as the UV/optical extinction curve, partly due to the substantial drop in extinction from

* zhenzhenshao@mail.bnu.edu.cn

† bjiang@bnu.edu.cn

‡ lia@missouri.edu

¹ For example, based on the absence of any substructures in the interstellar 9.7 μm feature which is broad, smooth, and featureless, Li & Draine (2001), Kemper et al. (2004), Li et al. (2008), and Potet et al. (2015) concluded that interstellar silicates are predominantly amorphous rather than crystalline.

the UV, optical to the IR. In the literature, one often relies on Mie theory together with the optical constants synthesized for “astronomical silicates” (Draine & Lee 1984) or the experimentally-measured optical constants of cosmic silicate analogues (e.g., see Jäger et al. 1994, Dorschner et al. 1995) to calculate the $9.7\ \mu\text{m}$ extinction profile from submicron-sized spherical silicate grains.² The optical constants of “astronomical silicates” at $\sim 8\text{--}13\ \mu\text{m}$ were constructed based on the Trapezium emission profile (Gillett et al. 1975) which peaks at $\sim 9.56\ \mu\text{m}$ and has a full width of half maximum (FWHM) of $\sim 3.45\ \mu\text{m}$ (Draine & Lee 1984).³ In contrast, the peak wavelength and FWHM of the $9.7\ \mu\text{m}$ silicate extinction feature calculated from those experimentally-measured optical constants vary with the silicate composition (e.g., pyroxene vs. olivine) and the iron content (e.g., see Jäger et al. 1994, Dorschner et al. 1995).⁴

Various efforts have been made to observationally determine the $9.7\ \mu\text{m}$ interstellar extinction feature. However, the results were somewhat contradictory. Kemper et al. (2004) analyzed the $\sim 8\text{--}13\ \mu\text{m}$ spectrum of the Galactic center source Sgr A* obtained with the *Short Wavelength Spectrometer* (SWS) on board the *Infrared Space Observatory* (ISO). The $9.7\ \mu\text{m}$ silicate absorption profile of Sgr A*, derived by subtracting a fourth-order polynomial continuum from the observed spectrum, peaks at $\sim 9.8\ \mu\text{m}$ and has a FWHM of $\sim 1.73\ \mu\text{m}$, much narrower than that of “astronomical silicates”. They suggested that the narrow profile could be caused by the contamination of the silicate emission intrinsic to the Sgr A* region. Chiar & Tielens (2006) obtained the $\sim 2.38\text{--}40\ \mu\text{m}$ *ISO*/SWS spectra of the diffuse ISM along the lines of sight toward four heavily extinguished WC-type Wolf-Rayet stars. They found that the $9.7\ \mu\text{m}$ silicate absorption features of those four sources all peak at $\sim 9.8\ \mu\text{m}$, but their widths vary from $\sim 2.35\ \mu\text{m}$ for WR 98a to $\sim 2.7\ \mu\text{m}$ for WR 104.

McClure (2009) derived the $\sim 5\text{--}20\ \mu\text{m}$ extinction curves for 28 G0–M4 III stars lying behind the Taurus, Chameleon I, Serpens, Barnard 59, Barnard 68 and IC 5146 molecular clouds. This was achieved by comparing the spectrum of each object obtained with the *Infrared Spectrograph* (IRS) on board the *Spitzer Space Telescope* with the stellar photospheric model spectrum of Castelli et al. (1997). She found that the $9.7\ \mu\text{m}$ silicate extinction feature appears to be broadened in more heavily extinguished regions: on av-

erage, in regions with $A_{K_S} < 1\ \text{mag}$,⁵ it peaks at $\sim 9.63\ \mu\text{m}$ and has a FWHM of $\sim 2.15\ \mu\text{m}$; in contrast, in regions with $1 < A_{K_S} < 7\ \text{mag}$, it peaks at $\sim 9.82\ \mu\text{m}$ and has a FWHM of $\sim 2.72\ \mu\text{m}$. Olofsson & Olofsson (2011) derived the mid-IR extinction curve for a highly obscured M giant (# 947) behind the dark globule B 335 ($R_V \approx 4.9$, $A_V \sim 10\ \text{mag}$), using the $\sim 7\text{--}14\ \mu\text{m}$ *Spitzer*/IRS spectrum complemented by the $\sim 5\text{--}16\ \mu\text{m}$ spectrum obtained with the ISOCAM/CVF instrument on board *ISO*. They found that the $9.7\ \mu\text{m}$ silicate extinction feature peaks at $\sim 9.2\ \mu\text{m}$ and has a FWHM of $\sim 3.80\ \mu\text{m}$. Also based on the *Spitzer*/IRS data, van Breemen et al. (2011) investigated the silicate absorption spectra of three sightlines toward diffuse clouds and four sightlines toward the Serpens, Taurus and ρ Ophiuchi molecular clouds. They found that the $9.7\ \mu\text{m}$ silicate absorption bands in the diffuse sightlines show a strikingly similar band shape and all closely resemble that of Sgr A* (Kemper et al. 2004), while the $9.7\ \mu\text{m}$ features in the molecular sightlines differ considerably from that of Sgr A* by peaking at $\sim 9.72\ \mu\text{m}$ and having a FWHM of $\sim 2.4\ \mu\text{m}$. More recently, Fogerty et al. (2016) analyzed the *Spitzer*/IRS spectra of the $9.7\ \mu\text{m}$ silicate optical depths of the diffuse ISM along the lines of sight toward Cyg OB2 No. 12, a heavily extinguished luminous B5 hypergiant with $A_V \approx 10.2\ \text{mag}$, and toward ζ Ophiuchi, a lightly extinguished bright O9.5 star with $A_V \approx 1\ \text{mag}$. They found appreciable differences between the spectral profile of the $9.7\ \mu\text{m}$ silicate absorption of Cyg OB2 No. 12 and that of ζ Ophiuchi: while the former peaks at $\sim 9.74\ \mu\text{m}$ and has a FWHM of $\sim 2.28\ \mu\text{m}$, the latter peaks at $\sim 9.64\ \mu\text{m}$ and has a FWHM of $\sim 2.34\ \mu\text{m}$. Moreover, the contrast between the feature and the absorption continuum of the former exceeds that of the latter by $\sim 30\%$.

In this work, we shall make use of the *Spitzer*/IRS spectra of early-type O and B stars to derive the $9.7\ \mu\text{m}$ interstellar silicate extinction feature. Differing from previous works, we will utilize the “pair” method, i.e., we will compare the *Spitzer*/IRS spectra of two stars of similar spectral types, with one star being obscured by interstellar dust while the other star unaffected by dust. In §2 we present the sample selection and in §3 we describe the extinction determination method. The results are presented and discussed in §4 and summarized in §5.

2 THE SAMPLE

Typically, red giants are used to trace the interstellar extinction in the IR (e.g., see Indebetouw et al. 2005, Flaherty et al. 2007, Gao et al. 2009, Zasowski et al. 2009, Majewski et al. 2011, Wang et al. 2013, Yuan et al. 2013, Davenport et al. 2014, Xue et al. 2016). This is because red giants are so bright that they are still “visible” in the IR even if they are severely obscured in the UV/optical. However, red giants are not suitable for studying the $9.7\ \mu\text{m}$ interstellar silicate extinction feature since the gas-phase molecular absorption bands (e.g., the Si–O stretches of the SiO gas which extend from $\sim 8\ \mu\text{m}$ to $\sim 11\ \mu\text{m}$) intrinsic to red giants could contaminate the derivation of the interstellar silicate feature

² For submicron-sized silicate grains, the calculated $9.7\ \mu\text{m}$ extinction profile is insensitive to the exact grain size since they are in the Rayleigh regime (Bohren & Huffman 1983).

³ The Trapezium emissivity profile was chosen because it appears to provide a good fit to the then $9.7\ \mu\text{m}$ absorption band observed in dark clouds as well as emission by hot circumstellar dust around many oxygen-rich stars. Draine & Lee (1984) had already recognized that some stars with circumstellar emission do show a narrower $9.7\ \mu\text{m}$ emission feature, e.g., the circumstellar $9.7\ \mu\text{m}$ emission feature of μ Cephei (Roche & Aitken 1984), a red supergiant, peaks at $\sim 9.69\ \mu\text{m}$ and has a width of $\sim 2.35\ \mu\text{m}$.

⁴ It is well recognized that the peak wavelength of the $9.7\ \mu\text{m}$ extinction profile of silicate dust depends on the level of SiO₄ polymerization, e.g., it shifts from $\sim 9\ \mu\text{m}$ for pure SiO₂ to $\sim 9.7\ \mu\text{m}$ for MgSiO₃ to $\sim 10.25\ \mu\text{m}$ for Mg_{2.4}SiO_{4.4} (Jäger et al. 2003, Henning 2010).

⁵ McClure (2009) assumed $R_V = 5$ which corresponds to $A_V \approx 7.75 A_{K_S}$.

(e.g., see van Breemen et al. 2011). In contrast, early-type stars are usually free of circumstellar dust and are bright in the IR. Also, their stellar photospheric emission in the IR can be closely characterized by the Rayleigh-Jeans law. Therefore, the determination of the stellar emission in the IR of early-type stars is relatively straightforward and accurate. In this work, we shall choose early-type (O and B) stars as the tracers of the interstellar silicate extinction profiles.

To date, $\sim 17,000$ low-resolution spectra have been obtained by *Spitzer*/*IRS*. These spectra were merged from four slits: SL2 ($\sim 5.21\text{--}7.56\ \mu\text{m}$), SL1 ($\sim 7.57\text{--}14.28\ \mu\text{m}$), LL2 ($\sim 14.29\text{--}20.66\ \mu\text{m}$), and LL1 ($\sim 20.67\text{--}38.00\ \mu\text{m}$). Chen et al. (2016) cross-identified the types of these objects in the *SIMBAD* database, supplemented with the photometric results from the *2MASS* and *WISE* all-sky surveys. This cross-identification resulted in a database of 71 O stars, 271 B stars and 374 A stars. We take the following approach to select our sample:

- We first exclude those showing silicate and/or polycyclic aromatic hydrocarbon (PAH) emission features. Although early-type stars are generally free of circumstellar dust, some B- and A-type stars could host a protoplanetary or debris disk which could emit at the 9.7 μm silicate feature (and even crystalline silicate features at 11.3, 18, 23, 28, 33, 40 and 60 μm ; see Henning & Meeus 2011) and/or the 3.3, 6.2, 7.7, 8.6, and 11.3 μm PAH features (see Seok & Li 2017). This procedure leads to the rejection of 38 stars which show amorphous and/or crystalline silicate features and seven stars showing PAH features.

- We require the signal-to-noise ratio (S/N) of the *Spitzer*/*IRS* spectrum to exceed 30. Because of this requirement, we are left with 48 O stars, 214 B stars and 316 A stars.

- To avoid saturation, for a star to be selected, we require it to be fainter than 5 mag in the *2MASS* K_S band, which is taken as the reference band for measuring the color excess. Because of this, Cyg OB2 No. 12 (an O star with a nominal *2MASS* K_S -band magnitude of ~ 2.70 mag) and ζ Ophiuchi (a B star with a nominal K_S magnitude of ~ 2.62 mag), which were used to trace the interstellar silicate extinction in Fogerty et al. (2016), are not included in our sample since they are much brighter than the saturation limit of ~ 5 mag in K_S .

- To make sure that the line of sight is obscured sufficiently so that the 9.7 μm silicate extinction is appreciable, we require the color index $J - K_S$ to exceed 0.4 mag, corresponding to a line-of-sight extinction of $A_{K_S} > 0.2$ mag, which is comparable to three times of the photometric error.

While the peak extinction of the 9.7 μm silicate feature is comparable to A_{K_S} , the extinction of the blue and red wings of the 9.7 μm silicate feature drops by a factor of > 2 (e.g., see Xue et al. 2016). With $A_{K_S} > 0.2$ mag, the entire 9.7 μm silicate extinction profile should be measurable.

The above selection process leads to the selection of some A stars. However, it turns out that those stars have systematically small color excess $E(J - K_S)$ and weak silicate absorption. We therefore decide to drop all those A stars. Also, the free-free emission of supergiants, arising from stellar winds of hot plasma, may potentially deform the slope of the stellar emission in the IR and thus affect the derivation

of the interstellar extinction curve.⁶ In the wavelength range of *Spitzer*/*IRS*, the ionized wind reveals itself through the 7.5 μm Pfund α and 12.4 μm Humphries α emission lines of hydrogen. Therefore, we exclude these stars which exhibit the 7.5 μm Pf α and 12.4 μm Hu α emission lines. As a result, the final sample consists of five stars (i.e., one O star and four B stars). Their locations in the Galaxy, spectral types, brightness in the *2MASS* and *WISE* bands are listed in Table 1. Also tabulated in Table 1 is $Err(J - K_S)$, the uncertainty of the *2MASS* $J - K_S$ color index, which is at most ~ 0.03 mag for all the sightlines. The *Spitzer*/*IRS* spectra of the selected stars are taken from the Cornell Atlas of *Spitzer*/*IRS* Sources (CASSIS; Lebouteiller et al. 2011). The CASSIS atlas provides *Spitzer*/*IRS* spectra reduced using a dedicated spectral extraction pipeline which performs optimal extraction for point-like sources and a regular extraction for partially extended sources. A comparison with the spectra reduced from the *Spitzer*/*IRS* pipeline shows that the CASSIS spectra are better calibrated (e.g., the negative flux which frequently shows up in the *Spitzer*/*IRS* pipeline spectra essentially never shows up in the CASSIS spectra).

Since the flux calibration of the CASSIS spectra largely affects the reliability of the derived silicate extinction feature, we also use the IR photometric data from *WISE*, *Spitzer*/*IRAC* and *AKARI* to check the credibility of the CASSIS spectra. For each of our five target stars, we search for the photometric data in the four *WISE* bands at 3.35, 4.60, 11.56 and 22.08 μm for W1, W2, W3 and W4, respectively; the four *Spitzer*/*IRAC* bands at 3.55, 4.49, 5.73 and 7.87 μm for IRAC1, IRAC2, IRAC3, and IRAC4, respectively; and the two *AKARI* bands at 8.23 and 17.61 μm for S9W and L18W, respectively. The photometric data of the selected sources are listed in Table 2. As shown in Figures 1, 2, the photometry and spectroscopy of our five target stars as well as two reference stars (see §3) are highly consistent. This also indirectly manifests that there is no light variation for these sources since the photometry and spectroscopy were not performed at the same epoch. The only exception is the W4-band photometry of StRS 164 which only yields an upper limit. Also, the *Spitzer*/*IRS* flux of StRS 164 is negative at $\lambda > 20.5\ \mu\text{m}$. This implies that the measurement at $\lambda \gtrsim 20.5\ \mu\text{m}$ may not be reliable for StRS 164. In Table 2, we label the W4-band flux of StRS 164 with “.”, which means “uncertain”. Nevertheless, all the sources show high consistency between photometry and spectroscopy at $\lambda < 15\ \mu\text{m}$ (i.e., the wavelength range of the *Spitzer*/*IRS* SL1 and SL2). As a result, the determination of the 9.7 μm silicate extinction profile is apparently more reliable than the 18 μm profile. In this work, we shall focus on the extinction at $\lambda < 15\ \mu\text{m}$.

⁶ Barlow & Cohen (1977) reported the detection of IR excess at wavelengths longward of $\sim 10\ \mu\text{m}$ in O supergiants and attributed it to free-free emission. Also, to account for the free-free emission from the stellar wind of the B5 hypergiant Cyg OB2 No. 12, Fogerty et al. (2016) added an $\lambda^{-0.6}$ component in the IR spectrum.

3 METHOD

The interstellar UV/optical extinction curve is often determined by comparing the spectrum of a reddened star with that of an un-reddened star of the same spectral type. We take a similar approach for the $9.7\ \mu\text{m}$ silicate extinction.

The apparent stellar spectrum F_λ is the intrinsic spectrum F_λ^0 dimmed by the interstellar extinction A_λ and the geometrical distance d :

$$F_\lambda = \frac{F_\lambda^0 \cdot \exp(-A_\lambda/1.086) \cdot \pi r^2}{4\pi d^2}, \quad (1)$$

where r is stellar radius. If the reference star has the same intrinsic spectrum as the target star, then the intrinsic flux ratio of the star at K_S and λ can be substituted by that of the reference star, i.e., $F_{K_S}^0/F_\lambda^0 = F_{K_S}^{\text{ref}}/F_\lambda^{\text{ref}}$, where “ref” refers to the reference star. By comparing the observed spectrum of the source star with the apparent spectrum of the reference star, we obtain $E(\lambda - K_S)$, the color excess between λ and the K_S band, as

$$\begin{aligned} E(\lambda - K_S) &= A_\lambda - A_{K_S} = -2.5 \log \left(\frac{F_\lambda}{F_{K_S}} \frac{F_{K_S}^{\text{ref}}}{F_\lambda^{\text{ref}}} \right) \\ &= -2.5 \log \left(\frac{F_\lambda}{F_\lambda^{\text{ref}}} \right) + 2.5 \log \left(\frac{F_{K_S}}{F_{K_S}^{\text{ref}}} \right) \\ &= -2.5 \log \left(\frac{F_\lambda}{F_\lambda^{\text{ref}}} \right) + m_{K_S}^{\text{ref}} - m_{K_S}, \end{aligned} \quad (2)$$

where m_{K_S} and $m_{K_S}^{\text{ref}}$ are respectively the apparent K_S -band magnitudes of the source star and the reference star. Since we are considering the color excess $E(\lambda - K_S)$ instead of the extinction A_λ , we do not need to know the distance d to the source star (or the reference star) as it gets cancelled out in eq. 2.

For each source star, we need to find a reference star which is not subject to any interstellar extinction but has the same intrinsic spectrum in the *Spitzer*/IRS wavelength range. In principle, an unreddened star of the same spectral type *and* the same luminosity class would be the best choice. For this purpose, we first attempt to select unreddened O and B stars by requiring the observed color index $J - K_S$ to be smaller than 0, i.e., bluer than an A0 star.⁷ However, this turns out to be impractical as it is difficult to find a reference star of the same spectral type and the same luminosity class for every source star. Specifically, all the source stars selected in this work are supergiants except HD 147701 which is classified as a giant, while most of the stars with $J - K_S < 0$ are dwarfs. Therefore, it is desirable to somewhat relax the criteria: perhaps a reference star could be selected based on its spectral type *or* luminosity class alone? To this end, we explore which plays a more important role, the luminosity class or the spectral type, in affecting the slope of the stellar continuum in the IR, by comparing the stellar emission spectral energy distribution in the wavelength range of *Spitzer*/IRS for stars of the same luminosity class or of the same spectral type. As illustrated in Figure 3, the spectral slope of a B0V star in the wavelength range of $\sim 5\text{--}38\ \mu\text{m}$ closely resembles that of a B8V star. In contrast, the spectral slope of a B0V star considerably differs from that of a B0I star. This demonstrates that

the luminosity class affects the IR slope of the stellar emission more significantly than the spectral type.⁸ Therefore, we choose HD 204172, a supergiant with $J - K_S \approx -0.056$ and $\alpha \approx 1.768$ (see Table 1), as the reference star for the four supergiants (i.e., one O supergiant and three B supergiants) among our five source stars,⁹ where $\alpha \equiv d \ln F_\nu^*/d \ln \nu$ is the slope of the $\sim 5\text{--}38\ \mu\text{m}$ stellar emission, where F_ν^* is the stellar flux at frequency ν . HD 147701, a B5III star, is the only target star in our sample which is not classified as a supergiant. We could not find any reference star with the same luminosity class as HD 147701.¹⁰ Therefore, we take HD 128207, a B8V star with $J - K_S \approx -0.056$ ¹¹ to be the reference star for HD 147701. Finally, we note that the integrated CO (1–0) line intensities along the lines of sight to HD 204172 ($\sim 0.03\ \text{K km s}^{-1}$) and HD 128207 ($\sim 0.04\ \text{K km s}^{-1}$) are rather small, as measured by *Planck* (see *Planck* Collaboration XIII 2014 and Table 1). This confirms that these reference stars experience no or negligible extinction.

There are some small-amplitude spikes in the *Spitzer*/IRS spectra of both reference and source stars due to noise, although some may be ionic or atomic lines. These small spikes cause appreciable fluctuations in the color excess because the color excess comes from the division of the two spectra where the error propagation amplifies the uncertainty. Since we are mostly interested in the silicate feature, we smooth the observed spectra in the following way: (i) for the reference stars, the spectra are fitted with a power law (see Figure 4); (ii) for the source stars, the spectra are fitted with a polynomial function (e.g., see Figure 5). In this way, we may lose the information of some dust species (e.g., ices), but the profile of the silicate extinction will be better determined.

4 RESULTS AND DISCUSSION

By comparing the *Spitzer*/IRS spectra of our five source stars with that of reference stars, we calculate the color excess $E(\lambda - K_S)$. We further normalize $E(\lambda - K_S)$ by $E(J - K_S)$ to cancel out the extinction quantity. In Figure 6 we show the color excess ratios $E(\lambda - K_S)/E(J - K_S)$ for our five sources. Most noticeably, the $9.7\ \mu\text{m}$ silicate extinction feature is pronounced in all five sources.

⁸ This actually can be understood in terms of the Rayleigh-Jeans approximation, i.e., the stellar spectral type or effective temperature (T_\star) has little effect on the IR slope of the stellar emission: $F_\lambda \propto \lambda^{-4} T$ provided $hc/(\lambda k T_\star) \ll 1$, where h is the Planck constant, c is the speed of light, and k is the Boltzman constant.

⁹ Koornneef (1983) measured the intrinsic color of B0I stars to be $J - K \approx -0.11$. This suggests that HD 204172 may suffer a reddening of $E(J - K_S) \approx 0.05\ \text{mag}$. Consequently, this may bring up a reddening of $E(\lambda - K_S) \approx 0.01\ \text{mag}$ in the *Spitzer*/IRS wavelength range, which is negligible.

¹⁰ We note that the classification of HD 147701 as a giant may be questionable since B5 stars are usually dwarfs or supergiants.

¹¹ This color index agrees rather well with that of Koornneef (1983) who measured $J - K \approx -0.04$ for B8V stars.

⁷ By definition, for A0 stars $J - K_S = 0$.

4.1 The 9.7 μm Silicate Extinction Profile

In Figure 7 we compare the extinction profiles of our five sources which are all normalized to their peak extinction at $\sim 9.7 \mu\text{m}$. It is apparent that the 9.7 μm silicate profiles exhibit appreciable variations in band width, with that of HD 147701 and StRS 164 being considerably wider than that of StRS 136 and StRS 354.

To be more quantitative, we determine the peak wavelength (λ_{peak}) and FWHM (γ_{sil}) of the 9.7 μm silicate extinction feature for each source by fitting the $E(\lambda - K_S)/E(J - K_S)$ color excess curve with a Gaussian function peaking around 9.7 μm combined with a linear function representing the continuum extinction underlying the silicate feature (see Figure 6).

We tabulate in Table 3 the fitted λ_{peak} and γ_{sil} parameters, and strengths ($S_{9.7}$) of the 9.7 μm silicate extinction profiles feature derived from Figure 6.

It is apparent that the FWHM of the 9.7 μm extinction feature varies among our five sources. It appears that they fall into two groups: $\gamma_{\text{sil}} \approx 2.0 \mu\text{m}$ for StRS 136, StRS 354 and HD 116119,¹² and $\gamma_{\text{sil}} \approx 3.0 \mu\text{m}$ for StRS 164 and HD 147701. This is consistent with the earlier findings of Roche & Aitken (1984, 1985) who found that, with $\gamma_{\text{sil}} \approx 2.4 \mu\text{m}$, the silicate extinction profiles along the lines of sight to diffuse clouds and to the Galactic center are narrow, resembling the circumstellar silicate emission profile of the supergiant μ Cep, while the silicate extinction profiles of dense molecular clouds, with $\gamma_{\text{sil}} \approx 3.4 \mu\text{m}$, are significantly broader, similar to the Trapezium emission profile. However, different results have also been reported in the literature. Rieke & Lebofsky (1985) derived $\gamma_{\text{sil}} \approx 3.2 \mu\text{m}$ for the 9.7 μm silicate extinction profile of the Galactic center sightlines toward three stars within $\sim 100''$ ($\sim 5 \text{ pc}$) of the Galactic center,¹³ which is much broader than that of Roche & Aitken (1985), obtained for several mid-IR sources within $\sim 2 \text{ pc}$ of the centre of the Galaxy. While Pegourie & Papoular (1985) determined $\gamma_{\text{sil}} \approx 2.2 \mu\text{m}$ for dense clouds, which is much narrower than that of Roche & Aitken (1984). See Figure 3 of Draine (1989) for a detailed comparison.

For our five sources, there does not seem to be any relation between γ_{sil} and the interstellar environment. Both highly reddened lines of sight for which $E(J - K_S) \approx 1.9 \text{ mag}$ (i.e., StRS 136, StRS 354) and a moderately obscured line of sight with $E(J - K_S) < 0.5 \text{ mag}$ (i.e., HD 116119) exhibit a narrow 9.7 μm silicate extinction profile. Similarly, a broad 9.7 μm profile is also seen in both highly extinguished star (i.e., StRS 164) and moderately reddened star (i.e., HD 147701). McClure (2009) found that the 9.7 μm silicate extinction profile broadens at larger extinction of $A_{K_S} > 1.0$,

based on a comparison of the *Spitzer*/IRS spectra of obscured G0–M4 stars with their stellar model atmospheric spectra. We note that some of her stars (e.g., M stars) may have intrinsic circumstellar silicate emission. Some of the sightlines considered here may trace dense clouds. The three most reddened sources (StRS 136, StRS 164 and StRS 354) have a color index of $J - K_S \sim 1.8 \text{ mag}$ which corresponds to $A_V \sim 10 \text{ mag}$. They possibly traverse some dense medium. Indeed, the integrated CO (1-0) line intensities from *Planck* observations (Planck Collaboration XIII 2014), $\sim 425 \text{ K km s}^{-1}$ and $\sim 186 \text{ K km s}^{-1}$, respectively, for the StRS 136 and StRS 164 sightlines, are about one order of magnitude higher than that of the other sightlines (see Table 1). As a matter of fact, these two sources have the largest color excess ratio at 9.7 μm , i.e., $E(9.7 \mu\text{m} - K_S)/E(J - K_S) \approx 0.076$ and 0.181 , respectively. On the other hand, the CO line intensity of the StRS 354 sightline is only $\sim 18.9 \text{ K km s}^{-1}$, one order of magnitude smaller than that of StRS 136 and StRS 164. With a much smaller color excess ratio, i.e., $E(9.7 \mu\text{m} - K_S)/E(J - K_S) \approx -0.073$, it is likely that StRS 354 traces diffuse medium and its large color excess may originate from a pile of diffuse clouds along the sightline. The sightlines toward HD 116119 and HD 147701 unambiguously trace diffuse medium. They exhibit a color index of $J - K_S \approx 0.40$ and $J - K_S \approx 0.48$, respectively, corresponding to $A_V \sim 2 - 3 \text{ mag}$ (see Table 1). They also show small integrated CO intensities (~ 6.0 and $\sim 13.5 \text{ K km s}^{-1}$ respectively).

Interestingly, the peak wavelengths of the 9.7 μm extinction feature of our five source stars are rather stable: $\lambda_{\text{peak}} \approx 9.73 \mu\text{m}$ for all the three sightlines with $\gamma_{\text{sil}} \approx 2.0 \mu\text{m}$, and $\lambda_{\text{peak}} \approx 9.84 \mu\text{m}$ for the two sightlines with $\gamma_{\text{sil}} \approx 3.0 \mu\text{m}$. Although it appears that λ_{peak} intends to slightly increase with γ_{sil} , this cannot be explained in terms of the grain size effect (e.g., for a broadening of $\Delta\gamma_{\text{sil}} = 1 \mu\text{m}$, “astronomical silicate” would shift the peak of the 9.7 μm profile by $\Delta\lambda_{\text{peak}} \approx 0.24 \mu\text{m}$; see Shao et al. 2017).

In Figure 8 we compare the 9.7 μm silicate extinction profiles of all five sources. It is apparent that the dispersion in λ_{peak} is rather small. The mean profile, obtained by averaging over all five sources, peaks at $\lambda_{\text{peak}} \approx 9.75 \mu\text{m}$ and has a width of $\gamma_{\text{sil}} \approx 2.2 \mu\text{m}$. In Figure 9 we compare the mean 9.7 μm extinction profile with that of the WD01 models for $R_V = 3.1$ and $R_V = 5.5$. The 9.7 μm profiles of the WD01 model (i.e., $\gamma_{\text{sil}} \approx 3.0 \mu\text{m}$ and $\lambda_{\text{peak}} \approx 9.51 \mu\text{m}$ for $R_V = 3.1$, and $\gamma_{\text{sil}} \approx 3.6 \mu\text{m}$ and $\lambda_{\text{peak}} \approx 9.45 \mu\text{m}$ for $R_V = 5.5$) are much broader and peak at a much shorter wavelength than the mean extinction profile derived in this work. This is not unexpected since the dielectric functions of “astronomical silicate” were synthesized based on the Trapezium emission profile which peaks at $\lambda_{\text{peak}} \approx 9.56 \mu\text{m}$ and has a width of $\gamma_{\text{sil}} \approx 3.45 \mu\text{m}$ (see Gillett et al. 1975, Draine & Lee 1984). Figure 10 compares the mean extinction profile of the 9.7 μm feature derived here (normalized to its maximum value) with that of Sgr A*, a Galactic center source (Kemper et al. 2004), WR 98a, a heavily extinguished Wolf-Rayet star (Chiar & Tielens 2006), Cyg OB2 No. 12, a heavily extinguished hypergiant (Fogerty et al. 2016), and those molecular clouds of McClure (2009) with $A_{K_S} < 1 \text{ mag}$. Figure 11 is the same as Figure 10, but with the continuum extinction underlying the 9.7 μm feature subtracted. It is apparent that the mean silicate profile derived in this work is appreciably

¹² The red wing of the 9.7 μm feature of HD 116119 is rather flat (see Figure 6) and the continuum extinction underneath the 9.7 μm feature could have been overestimated and thus the derived band width could have been somewhat underestimated (see Figure 7).

¹³ Rieke & Lebofsky (1985) computed the interstellar extinction law between 8 and 13 μm by assuming the $\sim 8 - 13 \mu\text{m}$ interstellar opacity profile to resemble the average of the emission spectra of μ Cep (Russell et al. 1975) and the Trapezium (Forrest et al. 1975) and adopting $A_V/\Delta\tau_{9.7} = 16.6$, where $\Delta\tau_{9.7}$ is the optical depth of the 9.7 μm silicate absorption.

broad than that of the GC source Sgr A*, no matter the underlying continuum extinction is subtracted or not. It is in close agreement with that of WR 98a and Cyg OB2 No. 12, both of which are typical diffuse lines of sight. In contrast, the $9.7\ \mu\text{m}$ silicate profile of McClure (2009) for molecular clouds with $A_{K_S} < 1\ \text{mag}$ peaks at $\lambda_{\text{peak}} \approx 9.63\ \mu\text{m}$, although its width ($\gamma_{\text{sil}} \approx 2.15\ \mu\text{m}$) is close to that of WR 98a, Cyg OB2 No. 12, and the one derived here. The discrepancy in the silicate absorption profiles may arise from grain size, shape, and more importantly, composition.

The extinction around the $9.7\ \mu\text{m}$ silicate feature, expressed as the color excess ratio at λ_{peak} , $E(\lambda_{\text{peak}} - K_S)/E(J - K_S)$, varies from ~ -0.1 to ~ 0.2 , with a mean ratio of $\langle E(\lambda_{\text{peak}} - K_S)/E(J - K_S) \rangle \approx 0.03 \pm 0.11$ (see Table 5). In comparison, the WD01 model predicts $E(\lambda_{\text{peak}} - K_S)/E(J - K_S) \approx -0.162$ for $R_V = 3.1$ and $E(\lambda_{\text{peak}} - K_S)/E(J - K_S) \approx -0.008$ for $R_V = 5.5$. As shown in Figure 9, the color excess ratio at λ_{peak} derived here agrees better with that of the WD $R_V = 5.5$ model. This is also true for the extinction ratio A_λ/A_{K_S} around the $9.7\ \mu\text{m}$ feature derived by Xue et al. (2016) from the photometric data of *Spitzer*/IRAC, *Spitzer*/MIPS and *WISE* in the sense that it better matches the WD01 $R_V = 5.5$ model (see Figure 20 in Xue et al. 2016). We attribute the variations in $E(\lambda_{\text{peak}} - K_S)/E(J - K_S)$ to grain size effects: for dense regions of $R_V = 5.5$, large grains of $\gtrsim 0.5\ \mu\text{m}$ will raise the continuum extinction underlying the $9.7\ \mu\text{m}$ silicate feature and thus increase $E(\lambda_{\text{peak}} - K_S)/E(J - K_S)$ and A_λ/A_{K_S} . Indeed, as mentioned earlier, StRS 136 and StRS 164, the two sightlines which exhibit the largest $E(\lambda_{\text{peak}} - K_S)/E(J - K_S)$ color excess ratios, likely traverse dense clouds as revealed by the high CO (1-0) line intensities. According to the newest catalog of the Galactic molecular clouds (Rice et al. 2016), there are molecular clouds very close to the sightlines toward StRS 136 and StRS 164. In addition, the variations among the fractional contributions of other dust components (e.g., carbon dust) to the continuum extinction underneath the $9.7\ \mu\text{m}$ silicate feature could also cause the variations of the color excess ratios at λ_{peak} : a higher fractional contribution of carbon dust to the continuum extinction could raise $E(\lambda_{\text{peak}} - K_S)/E(J - K_S)$.

Finally, we have also explored $A_V/\Delta\tau_{9.7}$ for our five sources. While it is relatively straightforward to derive $\Delta\tau_{9.7}$, the $9.7\ \mu\text{m}$ silicate absorption optical depth, from the observed, continuum-subtracted $9.7\ \mu\text{m}$ extinction profile, it is less straightforward to determine A_V , the visual extinction toward each of the source sightline. For each source star, we first calculate the $V - K_S$ color from its *2MASS* K_S magnitude and its *SIMBAD* V magnitude and then compare it with the intrinsic $(V - K_S)_0$ color from the Allen’s Astrophysical Quantities (Cox 2000) for standard stars of the same spectral and luminosity types. This allows us to estimate the color excess $E(V - K_S)$. If A_{K_S} is known, then one can derive A_V from A_{K_S} and $E(V - K_S)$: $A_V = A_{K_S} + E(V - K_S)$. We determine A_{K_S} from the $E(J - K_S)$ color excess based on the *2MASS* data and adopt $A_J/A_{K_S} = 2.72$ (Xue et al. 2017): $A_{K_S} \approx E(J - K_S)/1.72$. See Table 4 for the color and color excess data derived for our five source stars. In Table 3 we tabulate A_V , $\Delta\tau_{9.7}$, and $A_V/\Delta\tau_{9.7}$ for each source. It is apparent that, with an average ratio of $\langle A_V/\Delta\tau_{9.7} \rangle \approx 18.2$, they are in close agreement with that of the solar neighborhood diffuse ISM for which

$A_V/\Delta\tau_{9.7} \approx 18.5$ (Roche & Aitken 1984), but substantially exceeding that of the Galactic center ($A_V/\Delta\tau_{9.7} \approx 9$, Roche & Aitken 1985) and the dust torus around active galactic nuclei (AGN; $A_V/\Delta\tau_{9.7} \approx 5.5$, Lyu et al. 2015). This suggests that the silicate grains in the interstellar clouds toward our five source stars could be considerably smaller than that toward the Galactic center and the AGN dust torus (see Shao et al. 2017).

4.2 Interstellar or Circumstellar?

As described in §2, the target sources are selected by excluding those showing the emission features of circumstellar amorphous silicates, crystalline silicates, and PAHs. However, circumstellar amorphous carbon or graphite could be present without being detected since it is featureless in the IR (e.g., see Rouleau & Martin 1991, Draine 2016).¹⁴ Also, circumstellar silicate could be present but its emission is hidden by the interstellar silicate extinction. To examine whether our sources could be surrounded by circumstellar dust, we follow van der Veen & Habing (1988) who proposed that the ratio of the *IRAS* $12\ \mu\text{m}$ flux to the *IRAS* $25\ \mu\text{m}$ flux could be used as an effective diagnosis of the presence or absence of circumstellar dust. Unfortunately, none of our five target sources was detected in the *IRAS* 12, 25, 60 and $100\ \mu\text{m}$ bands. We therefore, instead, use the fluxes of the *WISE* W3 and W4 bands since they are closely similar to the *IRAS* 12 and $25\ \mu\text{m}$ bands. To this end, the criterion of van der Veen & Habing (1988) for the presence of circumstellar dust becomes $W3 - W4 > 1.0$ (Jarrett et al. 2011; Sjouwerman et al. 2009).¹⁵ As can be seen in Table 2, all our targets show $W3 - W4 < 0.3$ (except StRS 164 for which the *WISE* W4 flux may be uncertain), suggesting that our sources are free of circumstellar dust.

Xue et al. (2016) found that those stars with circumstellar silicate emission appear to display apparent color excess at $K_S - W3$ in the $J - K_S$ vs. $K_S - W3$ diagram (see Figure 19 in Xue et al. 2016). We show in Figure 12 the distribution of our five target stars in the $J - K_S$ vs. $K_S - W3$ diagram, together with the average extinction tendency derived by Xue et al. (2016). It is noteworthy that all our stars follow the average extinction law reasonably well, indicating that our sources are free of circumstellar dust.

4.3 Analytical Representation of the Extinction

We fit the extinction in the near-IR measured by Xue et al. (2016) and the extinction around the $9.7\ \mu\text{m}$ silicate band

¹⁴ Pure crystalline graphite has a weak feature at $\sim 11.52\ \mu\text{m}$ arising from the out-of-plane lattice resonance of graphite (Draine 1984). This feature has not been detected yet, e.g., by *ISO*/SWS or *Spitzer*/IRS. It may be observable with the MIRI spectrograph on *James Webb Space Telescope* (see Draine 2016).

¹⁵ For example, Cyg OB2 No. 12, a prototypical diffuse sightline and known to be free of circumstellar dust, shows $W3 - W4 \approx 0.4$.

derived here with the following formula:

$$A_\lambda/A_{K_S} = a_0 + a_1 \exp(-\lambda/\lambda_1) + a_2 \exp(-\lambda/\lambda_2) + \frac{a_3}{1 + \exp[-(\lambda - \lambda_3 + 0.5 w_1)/w_2]} \times \left\{ 1 - \frac{1}{1 + \exp[-(\lambda - \lambda_3 - 0.5 w_1)/w_3]} \right\} + \frac{a_4}{w_4 \sqrt{\pi/2}} \times \exp\{-2[(\lambda - \lambda_4)/w_4]^2\}, \quad (3)$$

where $a_0 = 0.41980$; $a_1 = 21.82920$, $\lambda_1 = 0.42007 \mu\text{m}$; $a_2 = 3.83330$, $\lambda_2 = 1.02373 \mu\text{m}$; $a_3 = 0.82771$, $\lambda_3 = 9.87221 \mu\text{m}$, $w_1 = 1.72679 \mu\text{m}$, $w_2 = 0.44642 \mu\text{m}$, $w_3 = 1.06985 \mu\text{m}$; $a_4 = 0.13066$, $\lambda_4 = 9.72506 \mu\text{m}$, and $w_4 = 0.81006 \mu\text{m}$. In Figure 13 we show the observationally determined IR extinction and the analytically fitted extinction. We should note that eq. (3) is valid for $0.9 \mu\text{m} \lesssim \lambda \lesssim 15 \mu\text{m}$ and should not be extrapolated to longer wavelengths since A_λ given by eq. (3) does not seem to decline more rapidly than $1/\lambda$ which is required by the Kramers-Kronig relation (see Draine 2004).

5 SUMMARY

We have selected one O-type and four B-type stars to trace the interstellar silicate extinction. For each star, we have determined the silicate extinction profile around $9.7 \mu\text{m}$ by comparing its *Spitzer*/*IRS* spectrum with that of unreddened reference star. Our principal results are as follows:

(i) The silicate extinction features of all our five sources peak around $\lambda_{\text{peak}} \sim 9.69\text{--}9.87 \mu\text{m}$, appreciably longer than that of “astronomical silicates”.

(ii) The width of the $9.7 \mu\text{m}$ silicate extinction feature appears to bifurcate into two groups, a narrow one with a FWHM of $\gamma_{\text{sil}} \approx 2.0 \mu\text{m}$ (for three stars) and a broad one with $\gamma_{\text{sil}} \approx 3.0 \mu\text{m}$ (for two stars). The width does not show any environmental dependence.

(iii) With $\lambda_{\text{peak}} \approx 9.75 \mu\text{m}$ and $\gamma_{\text{sil}} \approx 2.2 \mu\text{m}$, the mean $9.7 \mu\text{m}$ extinction profile, obtained by averaging over our five stars, closely resembles that of the diffuse interstellar medium along the lines of sight toward Cyg OB2 No. 12 for which $\lambda_{\text{peak}} \approx 9.74 \mu\text{m}$ and $\gamma_{\text{sil}} \approx 2.28 \mu\text{m}$ and WR 98a for which $\lambda_{\text{peak}} \approx 9.77 \mu\text{m}$ and $\gamma_{\text{sil}} \approx 2.35 \mu\text{m}$.

(iv) The mean ratio of the visual extinction to the $9.7 \mu\text{m}$ silicate absorption optical depth is $\langle A_V/\Delta\tau_{9.7} \rangle \approx 18.2$, in close agreement with that of the solar neighborhood diffuse ISM but substantially exceeding that of the Galactic center and the dust torus around AGNs.

(v) The color excess ratio at the peak wavelength of the $9.7 \mu\text{m}$ silicate feature, $E(\lambda_{\text{peak}} - K_S)/E(J - K_S)$, is somewhat higher for the lines of sight with a higher CO (1-0) line intensity. We interpret this in terms of grain size effects: in dense regions, the presence of large grains would raise the continuum extinction underlying the $9.7 \mu\text{m}$ feature and thus increase $E(\lambda_{\text{peak}} - K_S)/E(J - K_S)$.

(vi) An analytical formula is presented to parameterize the interstellar IR extinction.

ACKNOWLEDGEMENTS

We thank B.T. Draine, S. Gao and the anonymous referee for their very helpful comments and suggestions. This

work is supported by NSFC through Projects 11373015, 11533002, U1631104, and 973 Program 2014CB845702. This work made use of the data taken mainly by *Spitzer*/*IRS*, *WISE* and 2MASS.

REFERENCES

- Barlow, M. J., & Cohen, M. 1977, *ApJ*, 213, 737
- Bohren, C.F., & Huffman, D. R. 1983, *Absorption and Scattering of Light by Small Particles*, Wiley, New York
- Cardelli, J. A., Clayton, G. C., & Mathis, J. S. 1989, *ApJ*, 345, 245 (CCM)
- Castelli, F., Gratton, R. G., & Kurucz, R. L. 1997, *A&A*, 318, 841
- Chen, R., Luo, A., Liu, J. M., & Jiang, B.W. 2016, *AJ*, 151, 146
- Chiar, J. E., & Tielens, A. G. G. M. 2006, *ApJ*, 637, 774
- Cox, A. N. 2000, ed., *Allens Astrophysical Quantities*, Springer, New York
- Davenport, J. R. A., Ivezić, Ž., Becker, A. C., et al. 2014, *MNRAS*, 440, 3430
- Dorschner, J., Begemann, B., Henning, Th., Jaeger, C., & Mutschke, H. 1995, *A&A*, 300, 503
- Draine, B. T. 1984, *ApJL*, 277, L71
- Draine, B. T. 1989, in *Infrared Spectroscopy in Astronomy*, ed. B. H. Kaldeich (ESA Special Publication, Vol. 290; Noordwijk: ESA), 93
- Draine, B. T. 2003, *ARA&A*, 41, 241
- Draine, B. T. 2004, in *The Cold Universe*, ed. A. W. Blain et al. (Berlin: Springer), 213
- Draine, B. T. 2016, *ApJ*, 831, 109
- Draine, B.T., & Lee, H.M. 1984, *ApJ*, 318, 485
- Flaherty, K. M., Pipher, J. L., Megeath, S. T., et al. 2007, *ApJ*, 663, 1069
- Fogerty, S., Forrest, W., Watson, D. M., Sargent, B. A., & Koch, I. 2016, *ApJ*, 183, 71
- Forrest, W. J., Gillett, F. C., & Stein, W. A. 1975, *ApJ*, 195, 423
- Gao, J., Jiang, B. W., & Li, A. 2009, *ApJ*, 707, 89
- Gillett, F. C., Forrest, W. J., Merrill, K. M., Soifer, B. T., & Capps, R. W. 1975, *ApJ*, 200, 609
- Henning, Th., 2010, *ARA&A*, 48, 21
- Henning, Th., & Meeus, G. 2011, in *Physical Processes in Circumstellar Disks around Young Stars*, ed. P. J. V. Garcia (Chicago, IL: Univ. Chicago Press), 114
- Indebetouw, R., Mathis, J. S., Babler, B. L., et al. 2005, *ApJ*, 619, 931
- Jäger, C., Mutschke, H., Begemann, B., Dorschner, J., & Henning, Th. 1994, *A&A*, 292, 641
- Jäger, C., Dorschner, J., Mutschke, H., Posch, T., & Henning, Th. 2003, *A&A*, 408, 193
- Jarrett, T. H., Cohen, M., Masci, F., et al. 2011, *ApJ*, 735, 112
- Kemper, F., Vriend, W. J., & Tielens, A. G. G. M. 2004, *ApJ*, 609, 826
- Koornneef, J., 1983, *A&A*, 128, 84
- Lebouteiller, V., Barry, D. J., Spoon, H. W. W., et al. 2011, *ApJS*, 196, 8
- Li, A., & Draine, B. T. 2001, *ApJ*, 550, L213
- Li, A., Wang, S., Gao, J., & Jiang, B.W. 2015, in *Lessons from the Local Group*, ed. Freeman, K.C., Elmegreen, B.G., Block, D.L. & Woolway, M. (Springer: New York), 85 (arXiv: 1507.06604)
- Li, M. P., Shi, Q. J., & Li, A. 2008, *MNRAS*, 391, L49
- Majewski, S. R., Zasowski, G., Nidever, & D. L. 2011, *ApJ*, 739, 25
- Martin, P. G., & Whittet, D. C. B. 1990, *ApJ*, 357, 113
- McClure, M. 2009, *ApJ*, 693, L81
- Olofsson, S. & Olofsson, G. 2011, *A&A*, 534, 127

- Pegourie, B., & Papoular, R. 1985, A&A, 142, 451
- Poteet, C.A., Whittet, D.C.B., & Draine, B.T. 2015, ApJ, 801, 110
- Planck Collaboration XIII. 2014, A&A, 571, A13
- Rice, T.S., Goodman, A.A., Bergin, E.A., Beaumont, C., & Dame, T.M. 2016, ApJ, 822, 52
- Rieke, G. H., & Lebofsky, M. J. 1985, ApJ, 288, 618
- Roche, P. F., & Aitken, D.K. 1984, MNRAS, 208, 481
- Roche, P. F., & Aitken, D.K. 1985, MNRAS, 215, 425
- Rouleau, F., & Martin, P. G. 1991, ApJ, 377, 526
- Russell, R. W., Soifer, B. T., & Forrest, W. J. 1975, ApJL, 198, 41
- Seok, J. Y., & Li, A. 2017, ApJ, 835, 291
- Shao, Z. Z., Jiang, B. W., & Li, A. 2017, ApJ, 840, 27
- Sjouwerman, L. O., Capen, S. M., & Claussen, M. J. 2009, ApJ, 705, 1554
- van Breemen, J. M., Min, M., Chiar, J.E., et al. 2011 A&A 526, A152
- van der Veen, W. E. C. J., & Habing, H. J. 1988, A&A, 194, 125
- Wang, S., Gao, J., Jiang, B. W., Li, A., & Chen, Y. 2013, ApJ, 773, 30
- Wang, S., & Jiang, B. W. 2014, ApJ, 788, L12
- Weingartner, J. C., & Draine, B. T. 2001, ApJ, 548, 296 (WD01)
- Whittet, D. C. B. 2003, Dust in the Galactic Environment (2nd ed; Bristol: Institute of Physics Publishing)
- Xue, M. Y., Jiang, B. W., Gao, J., et al. 2016, ApJS, 224, 18
- Yuan, H. B., Liu, X. W., & Xiang, M. S. 2013, MNRAS, 430, 2188
- Zasowski, G., Majewski, S. R., Indebetouw, R., et al. 2009, ApJ, 707, 510

Table 1. Stellar parameters for the target and reference stars

Object	Type	l (degrees)	b (degrees)	S/N	$J - K_S$ (mag)	$Err(J - K_S)$ (mag)	W_{CO} (K km s $^{-1}$)	Note
StRS 354	O7	076.97	−00.64	57	1.88	0.03	18.95	target
StRS 136	B8I	000.04	−00.57	74	1.78	0.03	425.26	target
StRS 164	B8I	014.21	−00.00	69	1.78	0.03	185.70	target
HD 116119	B8Ia	306.62	+00.63	59	0.42	0.02	40.85	target
HD 147701	B5III(?)	352.25	+16.85	43	0.48	0.03	13.50	target
HD 204172	B0I	83.39	−9.96	47	−0.06	0.03	0.03	reference
HD 128207	B8V	323.84	+18.35	76	−0.06	0.03	0.04	reference

Table 2. IR photometry for the target and reference stars

Object	J 1.235 μm (mag)	H 1.662 μm (mag)	K _S 2.159 μm (mag)	W1 3.353 μm (mag)	IRAC1 3.507 μm (mag)	IRAC2 4.437 μm (mag)	W2 4.603 μm (mag)	IRAC3 5.628 μm (mag)	IRAC4 7.589 μm (mag)	AKARI9 8.228 μm (mag)	W3 11.561 μm (mag)	AKARI18 17.609 μm (mag)	W4 22.088 μm (mag)	Note
StRS 354	7.620	6.369	5.736	5.352			4.847			4.745	5.073		4.669	target
StRS 136	6.880	5.725	5.101	4.338	4.685	4.736	4.227	4.383	4.363	4.318	4.562	3.824	4.129	target
StRS 164	7.662	6.499	5.886	5.262		5.992	4.993	5.212	5.245	5.198	5.527		6.670:	target
HD 116119	6.121	5.876	5.697	5.599	5.728	5.548	5.351	5.518	5.478	5.307	5.488		5.276	target
HD 147701	6.668	6.378	6.186	6.046			5.956				6.137		5.886	target
HD 204172	6.085	6.080	6.141	6.140			6.056			6.001	6.041		5.736	reference
HD 128207	5.959	6.052	6.015	6.048			5.992			5.807	6.087		5.882	reference

†: The photometric data is somewhat uncertain.

Table 3. The peak wavelengths (λ_{peak}), FWHMs (γ_{sil}), strengths ($S_{9.7}$; see Figure 6) of the 9.7 μm silicate extinction profiles. Also tabulated are the visual extinction (A_V), the optical depth of the 9.7 μm absorption feature ($\Delta\tau_{9.7}$), and $A_V/\Delta\tau_{9.7}$.

Object	λ_{peak} (μm)	γ_{sil} (μm)	$S_{9.7}$	A_V (mag)	$\Delta\tau_{9.7}$	$A_V/\Delta\tau_{9.7}$	Reference
StRS 354	9.75	1.78	0.33	12.2	0.58	21.0	
StRS 136	9.69	2.11	0.42	11.9	0.71	16.8	
StRS 164	9.81	2.99	0.50	11.4	0.82	14.0	
HD 147701	9.87	3.07	0.35	3.01	0.17	17.7	
HD 116119	9.75	1.90	0.25	2.38	0.11	21.6	
Average	9.75	2.20	0.36			18.2	
WD01 ($R_V = 3.1$)	9.51	3.01				14.5	
WD01 ($R_V = 5.5$)	9.45	3.55				14.2	
WR 98a	9.77	2.35		12.4	0.78	15.9	Chiar & Tielens 2006
Cyg OB2 No. 12	9.74	2.28		10.2	0.59	17.3	Fogerty et al. 2016
GC Sgr A*	9.77	1.73					Kemper et al. 2004

Table 4. The $J - K_S$ and $V - K_S$ colors of our five source stars and the intrinsic $(J - K_S)_0$ and $(V - K_S)_0$ colors derived from the Kurucz model spectra for stars of the same spectral and luminosity type. Also tabulated are the color excesses $E(J - K_S)$ and $E(V - K_S)$.

Object	Type	$J - K_S^a$ (mag)	$(J - K_S)_0$ (mag)	$E(J - K_S)$ (mag)	$V - K_S^b$ (mag)	$(V - K_S)_0^c$ (mag)	$E(V - K_S)$ (mag)
StRS 354	O7	1.884	-0.056	1.94	10.229	-0.82*	11.049
StRS 136	B8I	1.779	-0.056	1.835	10.899	0.07	10.829
StRS 164	B8I	1.776	-0.056	1.832	10.414	0.07	10.344
HD 147701	B5III	0.482	-0.056	0.538	2.281	-0.42**	2.701
HD 116119	B8I	0.424	-0.056	0.48	2.173	0.07	2.103

a: Data taken from *2MASS*

b: Data taken from *SIMBAD*

c: Data taken from Cox(2000)

*: Intrinsic color index of O9I due to the lack of data for O7I-type stars

** : Intrinsic color index of B5V due to the lack of data for B5III-type stars

Table 5. Color excess ratios $E(\lambda - K_S)/E(J - K_S)$ for the *2MASS* H band and the *WISE* W1, W2, W3 and W4 bands and at λ_{peak} , the peak wavelength of the 9.7 μm silicate extinction profiles determined in this work. Also shown are the model ratios of WD01 for $R_V = 3.1$ and $R_V = 5.5$ as well as that of Xue et al. (2016).

Band Star	H	W1	W2	W3	W4	λ_{peak}
StRS 354	0.358	-0.197	-0.414	-0.290	-0.341	-0.073
StRS 136	0.373	-0.415	-0.430	-0.239	-0.309	0.076
StRS 164	0.368	-0.340	-0.441	-0.141	0.649	0.181
HD 147701	0.288	-0.322	-0.385	-0.225	-0.310	0.040
HD 116119	0.500	-0.202	-0.544	-0.227	-0.033	-0.069
Average	0.377	-0.295	-0.443	-0.224	-0.248	0.031
RMS	0.077	0.094	0.060	0.054	0.144	0.107
WD01 $R_V = 3.1$	0.392	-0.359	-0.494	-0.410	-0.531	-0.162
WD01 $R_V = 5.5$	0.331	-0.248	-0.354	-0.309	-0.501	-0.008
Xue et al. (2016)	0.348	-0.238	-0.312	-0.269	-0.370	

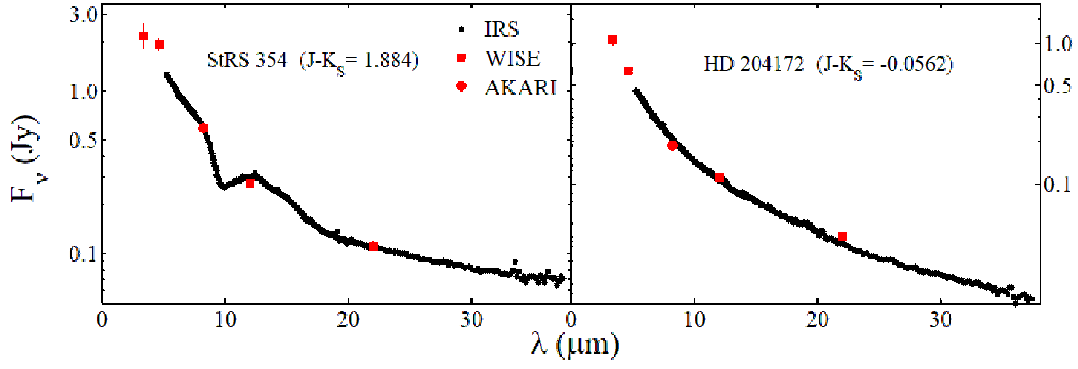


Figure 1. The *Spitzer*/IRS spectra and the IR photometry of the target O star StRS 354 and reference star HD 214680.

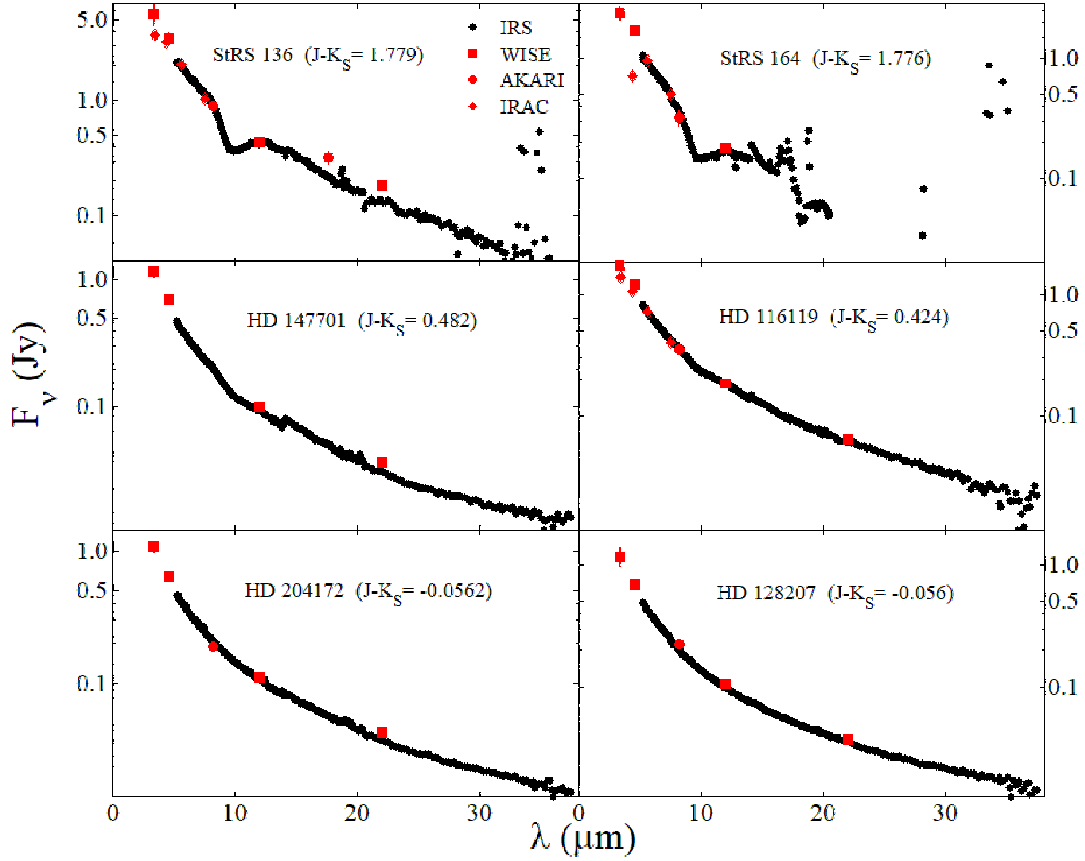


Figure 2. The *Spitzer*/IRS spectra and the IR photometry of the four target B stars (StRS 136, StRS 164, HD 147701 and HD 116119) and the two reference stars (HD 204172 and HD 128207).

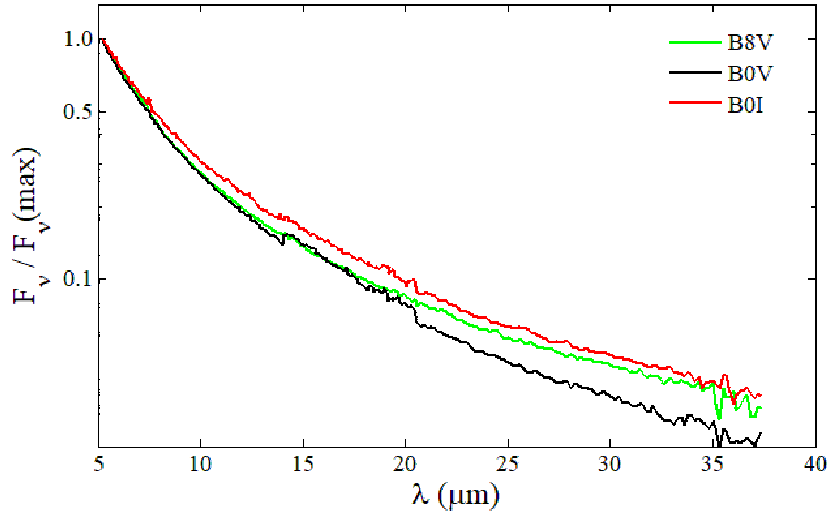


Figure 3. Comparison of the effects of the stellar spectral type on the IR slope of the stellar emission with that of the stellar luminosity class.

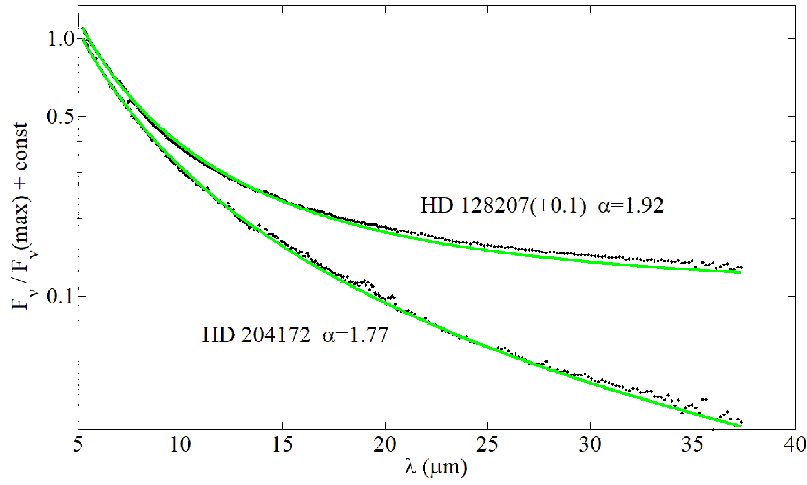


Figure 4. The *Spitzer*/*IRS* spectra (black dots) of the two reference stars (HD 128207 and HD 204172) and their power-law representation (i.e., $F_\nu \propto \nu^\alpha$).

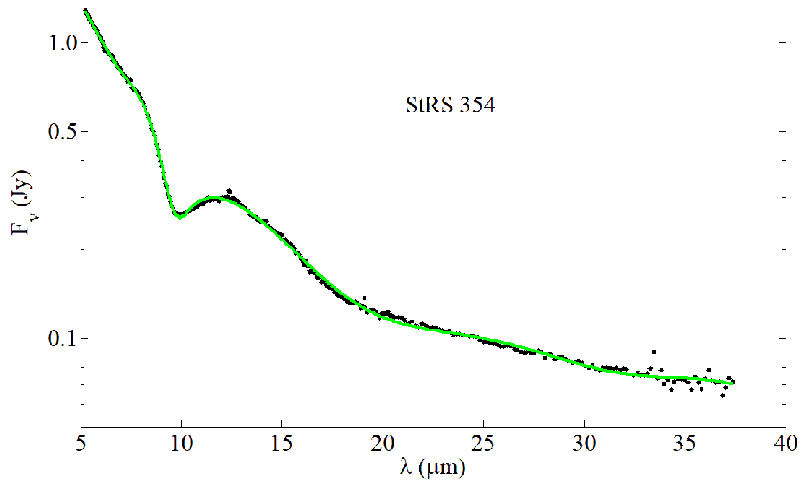


Figure 5. The *Spitzer*/*IRS* spectrum (black dots) of StRS 354, a target star, and its polynomial fit (green line).

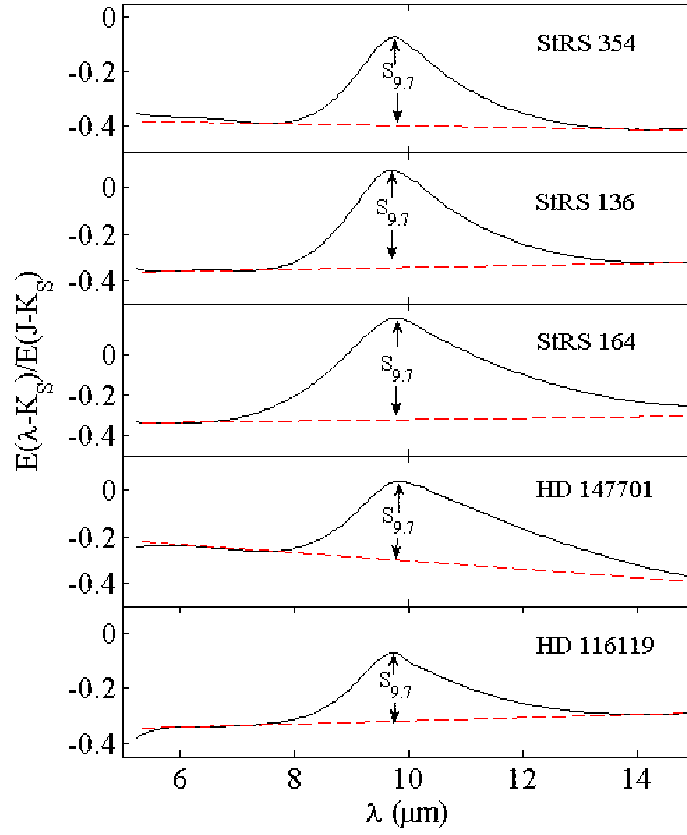


Figure 6. The $9.7\,\mu\text{m}$ silicate extinction profiles of our five target stars. Also shown is the underlying continuum extinction (dashed line).

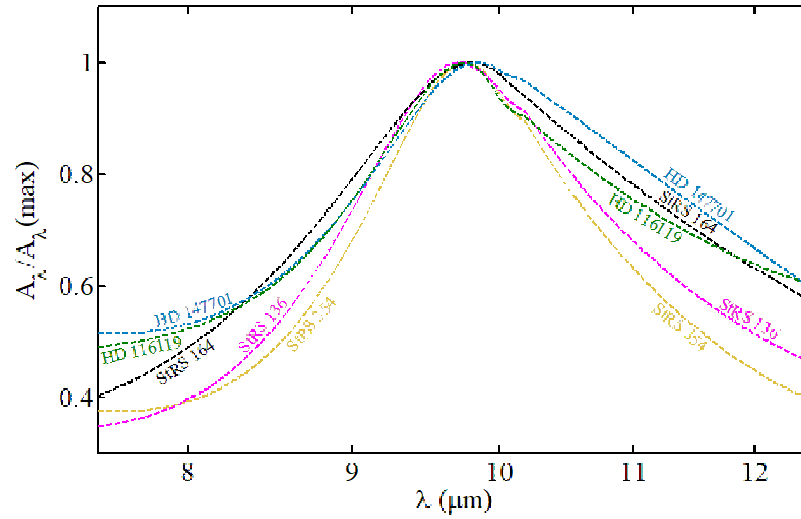


Figure 7. Comparison of the $9.7\,\mu\text{m}$ silicate extinction profiles of our five target stars shown in Figure 6. All profiles are normalized to their peak extinction at $\sim 9.7\,\mu\text{m}$.

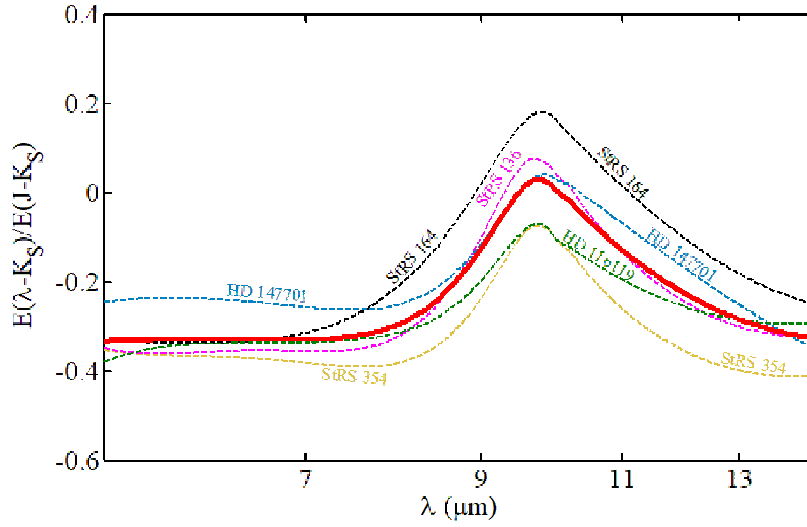


Figure 8. The $9.7\mu\text{m}$ silicate extinction profiles derived for the five target stars (broken line) and their average (thick solid red line).

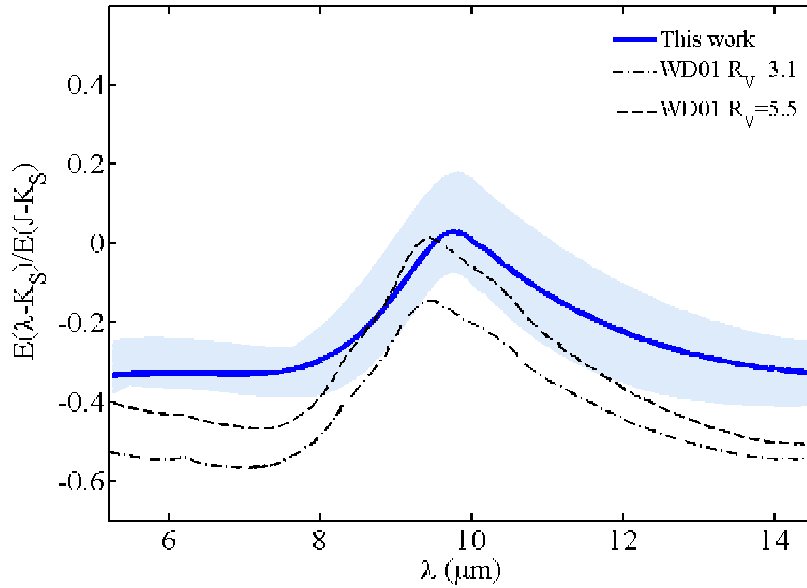


Figure 9. Comparison of the mean $9.7\mu\text{m}$ silicate extinction curve derived in this work (thick blue) with that of the WD01 model for $R_V = 3.1$ (dotted line) and for $R_V = 5.5$ (dashed line). The shaded region represents the variation range of the extinction derived here.

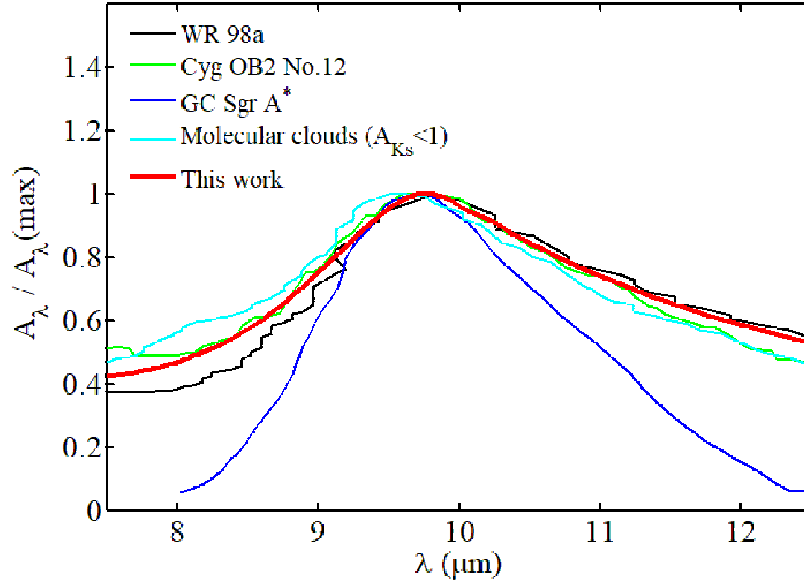


Figure 10. Comparison of the mean $9.7\,\mu\text{m}$ silicate extinction profile derived for the five early-type target stars (red line) with that of (i) the diffuse ISM toward WR98a (black line; Chiar & Tielens 2006), (ii) the diffuse ISM toward Cyg OB2 No.12 (green line; Fogerty et al. 2016), (iii) the Galactic Center sightline toward Sgr A* (blue line; Kemper et al. 2004), and (iv) molecular clouds of $A_{K_S} < 1$ mag (cyan line; McClure 2009).

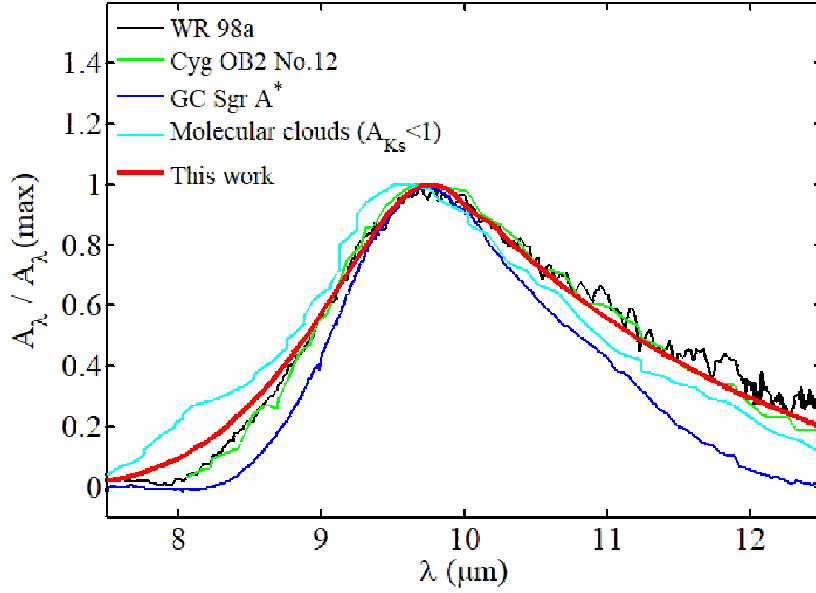


Figure 11. Same as Figure 10 but with the continuum extinction underlying the $9.7\,\mu\text{m}$ silicate feature subtracted.

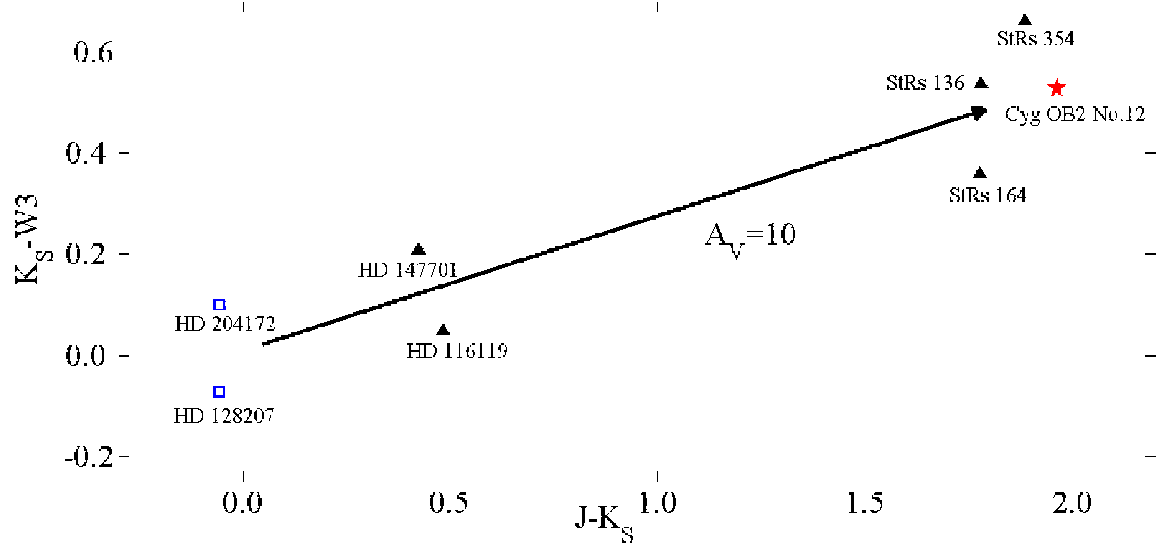


Figure 12. The $J - K_S$ vs. $K_S - W3$ diagram for the five target stars (triangles), two reference stars (open squares), and Cyg OB2 No. 12 (red star). The arrowed straight line denotes the extinction tendency for $A_V = 10$ mag (see Xue et al. 2016).

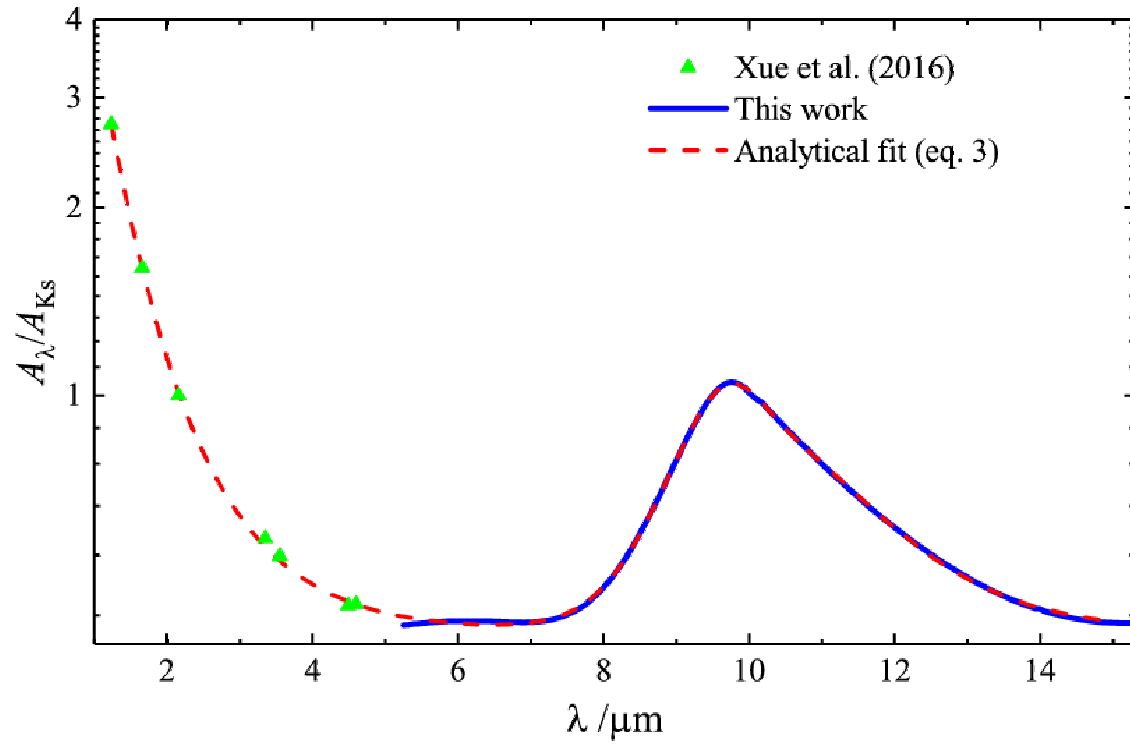


Figure 13. An analytical fit to the observed interstellar extinction curve in the IR at $0.9 \lesssim \lambda \lesssim 15 \mu\text{m}$.